Nat. Hazards Earth Syst. Sci. Discuss., 2, 4857–4887, 2014
www.nat-hazards-earth-syst-sci-discuss.net/2/4857/2014/
doi:10.5194/nhessd-2-4857-2014

Natural Hazards and Earth System Sciences
Open Access
Discussions

Simulating tsunami propagation in fjords with long wave models

F. Løvholt[1,2], S. Glimsdal[1,2], P. Lynett[3], and G. Pedersen[3]

[1]University of Oslo, Department of Mathematics, P.O. Box 1072, Blindern 0316, Oslo, Norway
[2]Norwegian Geotechnical Institute, P.O. Box 3930, 0806 Ullevål Stadion, Oslo, Norway
[3]Sonny Astani Department of Civil and Environmental Engineering, University of Southern California, Los Angeles, USA

Received: 12 July 2014 – Accepted: 15 July 2014 – Published: 1 August 2014

Correspondence to: F. Løvholt (finn.lovholt@ngi.no)

Published by Copernicus Publications on behalf of the European Geosciences Union.

Abstract

Tsunamis induced by rock slides constitute a severe hazard towards coastal fjord communities. Fjords are narrow and rugged with steep slopes, and modeling the short-frequency and high-amplitude tsunamis in this environment is demanding. In the present paper, our ability (and the lack thereof) to simulate tsunami propagation and run-up in fjords for typical wave characteristics of rock slide induced waves is demonstrated. The starting point is a 1 : 500 scale model of the topography and bathymetry of Storfjorden fjord system in western Norway. Using measured wave data from the scale model as input to numerical simulations, we find that the leading wave is moderately influenced by non-linearity and dispersion. For the trailing waves, dispersion and dissipation from the alongshore inundation on the traveling wave become more important. Tsunami inundation were simulated at the two locations of Hellesylt and Geiranger, providing good match with the measurements in the former location. In Geiranger, the most demanding case of the two, discrepancies are larger, which may in part be explained by scale effects, and in part combinations of errors emerging from both wave propagation along large stretches of the fjord and the inundation model itself.

1 Introduction

Subaerial landslides originating from subaerial rock slope failures are effective wave generators that impact the water body at high and initially supercritical speeds (see e.g. Fritz et al., 2004; Heller et al., 2008). They occur in fjords, lakes, or rivers, and with large volumes they may have significant tsunamigenic power. Examples of rock slide induced tsunamis include the 1961 Lituya Bay event (Miller, 1960), the Lago Yanahuin (Plafker and Eyzagiurre, 1979), the 1783 Scilla landslide (Tinti and Guidoboni, 1988), and in 2007 a series of rock slides in the Aisén fjord in southern Chile caused tsunamis that were documented on video (Sepúlveda and Serey, 2009). In Norway, three major tsunamis struck the communities in Loen (1904, 1936) and Tafjord (1934), causing

NHESSD
2, 4857–4887, 2014

altogether 175 fatalities (Jørstad, 1968; Harbitz et al., 1993). In Storfjorden, western Norway, a number of older rock slide events are evident from high resolution seabed surveys (Blikra et al., 2005). Some of the events are located immediately offshore the presently unstable Åknes rock-slope. Due to large relative movements up to 20 cm year^{-1} (Oppikofer et al., 2010) and unstable volumes exceeding several million m^3, Åknes is presently considered the most hazardous potential tsunamigenic rock-slope in Norway.

Fjords and narrow lakes may be effective wave guides as they channel the wave energy, involving less radial spread and scattering than for the tsunamis propagating in the open sea. Due to the impulsive nature of of the rock slide water impact, the wave evolution becomes dispersive. Traditional tsunami models based on the shallow water formulation (e.g. Titov and Synolakis, 1995; Imamura, 1996; Titov and Synolakis, 1997; LeVeque and George, 2008) do not include dispersion, and dispersive wave models such as those based on the Boussinesq formulation (Madsen and Sørensen, 1992; Nwogu, 1993; Wei et al., 1995; Lynett et al., 2002; Madsen et al., 2003) constitute better alternatives. Recently Boussinesq models have been formulated using the shock capturing approximate Riemann solvers in combinations with TVD limiters (Erduran et al., 2005; Kim et al., 2009; Kim and Lynett, 2011; Shi et al., 2012; Tonelli and Petti, 2012). Yet, recent work has demonstrated that the fjords constitute a demanding test case for Boussinesq models involving possible instabilities. The instabilities are for instance linked to the terms related to steep bathymetric slopes (Løvholt and Pedersen, 2009), or strong non-linearity and run-up (Løvholt et al., 2013). As a consequence the fully non-linear Boussinesq models with run-up are yet to be deployed for simulating tsunamis in fjords.

Due to the fjords being narrow and dominated by rugged steep slopes, tsunamis inundate the coastlines as they propagate. At the same time the tsunami may exhibit breaking. Both of the latter effects should be properly accounted for the in the propagation model, which obviously constitutes a challenge. Yet, such effects remain unquantified in the tsunami literature. Recently, Harbitz et al. (2014) simulated potential

NHESSD
2, 4857–4887, 2014

tsunamis in Storfjorden, using the dispersive wave model GloBouss (Pedersen and Løvholt, 2008; Løvholt et al., 2008). As run-up and breaking effects are not included in GloBouss, adaptation of the local bathymetry was necessary to facilitate the simulations. In the present paper, we investigate how these effects (run-up and breaking as well as non-linearity and dispersion, influence the wave propagation. The starting point is a 1 : 500 scale model of the topography and bathymetry of Storfjorden (Fig. 1). The experimental setup, which is rigorously explained by Lindstrøm et al. (2014), include a rigid landslide block source released at $t = 0$ s, immediately after impacting undisturbed water level, providing time series of the resulting surface elevations in the fjord basin. Using the time series, we here construct synthetic initial conditions that are used in different numerical models. By use of the measured time series to construct input conditions to our numerical models, we ensure amplitudes and wave periods mimicking those generated by a subaerial landslide. Employing the fully non-linear Coulwave model including run-up (Lynett et al., 2002; Kim et al., 2009; Kim and Lynett, 2011) and GloBouss (Pedersen and Løvholt, 2008; Løvholt et al., 2008) in various modes, we demonstrate the importance of various parameters and formulations on the wave propagation. We also study the run-up in the two fjord settlements of Hellesylt and Geiranger, using Coulwave and MOST coupled with GloBouss (Løvholt et al., 2010). Comparing the simulations with surface elevation measurements in control points located elsewhere in the scale model, we ensure that the wave amplitudes and wavelengths roughly comply with observations. Yet, it is strongly emphasized that the aim of the present work is to compare effects of different parameters and model formulations rather than accurately reproducing the laboratory data of Lindstrøm et al. (2014).

2 Employed Boussinesq models

We introduce a Cartesian coordinate system with horizontal axes, ox and oy in the undisturbed water level and an oz axis pointing vertically upward. The equilibrium depth is denoted by h, the surface elevation by η and the velocity components by u and v in

NHESSD
2, 4857–4887, 2014

the x and y directions, respectively. We identify a typical depth, d, a typical wavelength, L, and an amplitude factor, ϵ, which corresponds to a characteristic value of η/d. Different long wave equations can be obtained through perturbation expansions in $\mu \equiv d/L$ and ϵ. They may then be classified according to which orders these parameters are retained in the equations, when the equations are scaled such that the leading order is unity. The residual (error) terms of the standard Boussinesq equations, such as solved in the early Boussinesq models (Peregrine, 1967), are $O(\epsilon\mu^2, \mu^4)$. The primary unknowns then were the surface elevation and the vertically averaged horizontal velocity. Several other formulations with different choices of primary unknowns do exist, of which that of Nwogu (1993) has become widely used. In this formulation the velocity at a chosen depth z_α is used as a primary unknown. With the optimal choice $z_\alpha = -0.531\,h$ improved linear dispersion properties are obtained (good for wavelengths down to 2 h, say). Furthermore, Wei et al. (1995) presented a fully non-linear version of Nwogu's formulation, with residual terms akin to $O(|\nabla h|\mu^4, \mu^6)$. In the present paper, various kinds operational models retaining the residual terms to different degree based on the Boussinesq equations of the types listed above, are tested with respect to their ability to model tsunamis in fjords.

2.1 Fully non-linear operational model with run-up – Coulwave

The Coulwave long-wave model was first developed as a means to investigate waves generated by submarine landslides, and numerically was very similar to the initial versions of the FUNWAVE model Wei et al. (1995). Recently, the numerical scheme has been changed to utilize a finite-volume (FV) method for the Boussinesq equations in conservative (flux) form (Kim et al., 2009). Various turbulence and rotational effects have also been included (e.g. Kim and Lynett, 2011), but these features are not utilized here. Coulwave supports several different drying-wetting formulations (Lynett et al., 2010), and we here employ a centered run-up formulation (see e.g. Løvholt et al., 2013). The centered formulation is preferred due to better robustness and stability properties than the other formulations, on the expense of accuracy. On the open

NHESSD
2, 4857–4887, 2014

boundaries, a sponge layer is utilized. Unless otherwise stated, we run the Coulwave model in it's [illegible] mode and with a moving shoreline allowing for inundation. In certain occasions we also run the model assuming fixed shoreline position, or a [illegible]ing a non-dispersive (NLSW) version to address the model parameter sensitivity. For the NLSW case, a numerical finite difference formulation is used (Lynett et al., 2002).

A simplified internal source function based on measured surface elevations η_{lab} from wave gauges in the Åknes scale model (Fig. 1) is employed:

$$\eta_{\text{cw}}(x,y,t) = \alpha \cdot \Delta t \sum_{i=1}^{n} e^{-\beta \Delta y_i'^2} \cdot W_i(x_i') \cdot \eta_{\text{lab},i} \qquad (1)$$

Here η_{cw} is the surface elevation in the numerical model, and α and β are parameters that were tuned to provide a reasonable overall agreement with measurement data at the downstream gauge points. The summation indicate contributions from each of the gauge points i. For each gauge point, a bi-linear weight function W_i was employed along the orientation axis x_i' between two adjacent gauge points, i.e. being unitary at point i decaying linearly to points $i-1$ and $i+1$. Along the normal direction y_i', we applied the exponential weighting function. Thus, the formulation allows for including different time series gauges as a forcing function for the local numerical solution. Corresponding velocities were not available from the measurements. However, it is stressed that our emphasis is to study differences in model assumptions rather than reproducing the measured wave field.

Time series from three different bridges B, D, and F (Fig. 2) were used as input to internal source function (Eq. 1). The B bridge time series were used to provide joint inputs both for the Coulwave and GloBouss models, whereas the D and F time series were used for dedicated run-up studies in Coulwave only. Along the B bridge located relatively near the landslide source, we see that signals became [illegible] of phase already at the first wave cycle. As the out-of-phase contributions was found to set up strong artificial waves across the fjord, a single time series (B4) was instead applied for all the gauge points (B1–B8) along the B-bridge. Furthermore, two tapered versions of

NHESSD
2, 4857–4887, 2014

the B4 time series were used (Fig. 2, upper right), and instantaneous fields of resulting surface elevations and currents were outputted at times 5.07 and 7.1 s respectively (surface elevations are shown in Fig. 3), i.e. immediately after the wave forcing was stopped. These fields were used as initial conditions for the GloBouss simulations, hence enabling comparison between the results obtained by Coulwave and GloBouss. As discussed below, the tapering did not affect the leading wave evolution substantially. For bridges D and F phase difference were much less pronounced, and hence all the three time series across the bridges were utilized. As the time series gauges were aligned along almost straight lines, smooth input conditions were obtained.

Courant numbers of 0.1 were employed for the NLSW simulations, and 0.2 for the dispersive. Values of α and β were set to respectively $1.67\,\mathrm{m\,s^{-1}}$ and $17.8\,\mathrm{m^{-2}}$ for bridge B and F, and $0.41\,\mathrm{m\,s^{-1}}$ and $15.6\,\mathrm{m^{-2}}$ for bridge D. A spatially uniform friction factor $f = 0.005$ proportional to the square current velocity times inverse total water depth was used (see Lynett et al., 2002; Lynett, 2006, for details). As noted by Lynett et al. (2010), current velocities may become very large for small total water depths, and may cause instabilities. To counteract, Lynett et al. (2010) included a required minimum water depth needed to enable non-zero fluxes. Here, different minimum depths h_m are applied for different simulations. For the simulations covering the full bathymetry (using the B-bridge for the internal source function) we used a value of $h_m = 0.002\,\mathrm{m}$. For the dedicated run-up simulations in Coulwave (using the D and F-bridges for the internal source function) we could employ a smaller minimum depth of $h_m = 0.001\,\mathrm{m}$. We further used a transport based breaking criterion, a procedure adding advection to the conventional breaking model of Kennedy et al. (2000). For more details on the transport based breaking method, see Løvholt et al. (2013).

2.2 Mildly non-linear model for offshore wave propagation – GloBouss

GloBouss is a finite difference model formulated using the optimized standard Boussinesq equations (Pedersen and Løvholt, 2008; Løvholt et al., 2008), i.e. with dispersion properties identical to those of Nwogu (1993) and with second order non-linear terms.

NHESSD
2, 4857–4887, 2014

It is simpler and less computationally intensive than Coulwave, and may also be run both in linear shallow water or linear dispersive mode. This makes the model suitable for investigating the importance of the different features of the wave propagation. Here, GloBouss is run using the initial conditions provided from Coulwave using the tapered time series after $t = 5.07$ s and $t = 7.10$ s respectively.

GloBouss does not include drying-wetting and breaking formulations which is needed for simulating run-up. In their absence, non-linear terms in the Boussinesq models may lead to instability if the sea-bottom is exposed during simulation. This problem is especially severe in the generation area, but also for waves entering shallow water near shore. Numerically such problems are often handled by defining a so-called threshold depth. Implementation of such techniques is done either by replacing the data for the part of the bathymetry with depth smaller than the threshold value with the threshold value itself, or by moving the shoreline to the threshold depth. Here we have applied the first type with at threshold depth of 0.1 m.

Although GloBouss do not include moving shoreline and shock capturing facilities by itself, it is set up with a one-way nesting facility with the inundation model MOST (Titov and Synolakis, 1995, 1998). The surface elevation and velocities from GloBouss are fed into MOST are during the simulation over the boundaries, (see Løvholt et al., 2010, for details). The nesting is utilized below, and enables us to simulate the run-up in certain domains of interest such as Hellesylt and Geiranger. Here, MOST is run with the standard Manning friction parameter of $n = 0.03$ and a minimum depth of $h_m = 0.002$ m.

NHESSD
2, 4857–4887, 2014

3 Tsunami simulations in a scaled model fjord geometry

3.1 Comparing the Coulwave simulations with measured laboratory data

3.1.1 Fjord propagation

Figure 4 compares the simulated surface elevations using Coulwave with measurements (Lindstrøm et al., 2014) at the four different time series locations C2, D2, E2, and G2. We have used three different signals as input conditions at the B-bridge; the two tapered signals of B4 as well as a non-tapered signal. The comparisons show that using the non-tapered and the signal tapered at $t = 7.10$ s provide more or less identical results for at least the first 4–5 wave cycles. These two simulations also provide a somewhat better fit to the measurements compared to simulations using signal tapered at $t = 5.07$. The simulations generally compare well with the first wave, and capture the main trends in the preceding amplitudes and wave periods despite the clearly visible offsets. We therefore find that the tapered input conditions should provide realistic input conditions for the model comparisons, which is the emphasis of the present study.

A uniform grid resolution of $\Delta x = \Delta y = 0.126$ m was employed (which corresponds to a resolution of 63 m in full scale). In the present setting, model instability arose when the grid resolution was refined by a factor of two. As demonstrated by running the GloBouss model at higher resolution below, the present grid resolution is perhaps sufficiently accurate for the first 1–2 wave cycles, but becomes inaccurate for the trailing waves.

3.1.2 Near shore propagation and inundation

Figure 5 shows the location of measured onshore and offshore time series gauges located close to the fjord ends. These locations also comply with two of the closest settlements in Storfjorden, namely Hellesylt and Geiranger. Here, we use the time series

NHESSD
2, 4857–4887, 2014

gauges D1–3 and F1–3 provide input conditions for run-up simulations in Hellesylt and Geiranger respectively.

Figure 6 compares the simulated surface elevations and flow depths using Coulwave with the measurements by Lindstrøm et al. (2014) at four different time series locations in Hellesylt. Two different grid resolutions 0.11 m and 0.056 m were used. A relatively good match with the measured time series was obtained for the first run-up for all points. The main trends in the trailing waves are also captured, although clearly less accurate. While the offshore points show good convergence, deviations between the different grid resolutions are evident for the onshore points.

Figure 6 compares the simulated flow depths using Coulwave with measurements (Lindstrøm et al., 2014) at four different time series locations in Geiranger. Two different grid resolutions 0.126 m and 0.063 m were used. Here, the simulations match the measurements less accurately than in Hellesylt, particularly for two of the innermost locations (UG5–6). While the overall trend in the time series is captured at the finest resolution, the simulations shows that both employed resolutions are probably too coarse. The runs at finer resolutions were unstable prior to the maximum run-up.

3.2 Influence of hydrodynamic parameters on the wave evolution

3.2.1 Grid refinement tests

Grid refinement tests were conducted for the GloBouss model, including the nested simulations with MOST. This enables us to evaluate the accuracy of the models both for the leading and trailing wave systems. Being simpler, GloBouss can be run at higher resolution than Coulwave without encountering instabilities. Although the convergence is monitored mainly for GloBouss, it gives some indication also for Coulwave. The Coulwave simulations presented in this paper are run at the finest resolution allowed by the model to avoid instability.

The convergence is tested by comparing the surface elevation at locations D2 and E2, and UG1 and UH6, for the propagation phase (GloBouss) and run-up (MOST)

NHESSD
2, 4857–4887, 2014

respectively, see Figs. 8 and 9. For the propagation phase (Fig. 8), the finest resolution we have tested is 0.063 m. The GloBouss model is run in non-linear optimized dispersive mode. The initial condition is the solution tapered at 7.10 s. For the leading waves the difference in the surface elevation measured against the finest resolution is ranging from 3–4 % for the 0.126 m resolution. From this we may conclude that for the propagation phase the resolution of 0.252 m or finer is sufficient for proper convergence for the leading wave, and a resolution of 0.126 m for the second wave. For the further trailing wave system, we see that even finer resolutions are required for sufficient accuracy. Furthermore, we note that also GloBouss face instabilities at the highest grid resolution, indicated indirectly by the termination of the blue curve in Fig. 8.

Grid refinement tests for MOST model nested with GloBouss were conducted for the grid resolutions 0.01 m, 0.03 m and 0.063 m. Flow depths are depicted in Fig. 9. As shown, the solutions seem to converge slowly, with high frequency oscillations at the lowest grid resolution. Hence a high resolution of about 0.03 m is needed for a relatively good convergence, although a resolution of 0.01 m is needed to reproduce the smooth solution evident from the measurements. Both UG1 at Geiranger and UH6 at Hellesylt is located on dry land. For the Coulwave simulations in Hellesylt (see Fig. 6), solutions seems to converge more rapidly, however corresponding convergence is poor in Geiranger (see Fig. 7).

3.2.2 Fjord propagation

Using the B4 signal tapered at $t = 5.07$ s we run the Coulwave model for a $\Delta x = \Delta y = 0.126$ m grid resolution. Simulations were conducted using fully dispersive and NLSW formulations, both for a moving or fixed boundary. In the latter case, use of limiters and shock capturing terms still ensured model stability without alteration of the bathymetry. Correspondingly, GloBouss was run both in non-linear dispersive and linear mode at identical grid resolution. In both cases, optimized dispersion was used, although higher order dispersion was found negligible (results not shown). In the absence of breaking and shock capturing facilities, the bathymetry was altered as described in Sect. 2.2

NHESSD
2, 4857–4887, 2014

to ensure model stability. In GloBouss, we use the initial condition produced by the Coulwave model as shown in Fig. 3a.

Figure 10 compares the Coulwave and GloBouss simulations at the four different wave gauges. In the upper two panels, comparisons for relatively short propagation times are depicted at the gauges D2 and E2 located immediately after the fjord T-bend (see Fig. 1). For the leading wave at D2, we find only minor discrepancies between the models where the dispersive terms are retained, with 5% leading amplitude discrepancy between non-linear GloBouss and Coulwave. Correspondingly, the linear dispersive GloBouss simulation has a 7% amplitude discrepancy compared to the non-linear solution, but the arrival time is clearly shifted. The non-dispersive solution is easily distinguishable from the dispersive, with earlier arrival time and a shorter wave length. However, the hydrostatic solution (labeled NLSW in the figure), provides a surprisingly good fit to the leading wave. For E2, we also see that the leading NLSW solution do not display the smooth shape that is typical due to dispersion. For the preceding wave-train, individual model differences become more distinct. As expected, the NLSW model generally provide shorter and less regular wave components than the models containing dispersion. Compared to the Boussinesq runs, higher amplitude waves are found in the wave-train resulting from the linear dispersive simulations. In the Coulwave simulations with fixed shoreline, the wave is clearly more damped than for the case with moving shoreline, which may indicate that invoked breaking terms provide additional dissipation. Running the GloBouss model (without dissipation), the opposite is obtained, namely somewhat higher waves. In other words, there is a tendency that the non-linear dispersive Coulwave simulations provide somewhat smaller amplitude wave-trains than the GloBouss model. We may not immediately recognize from where the discrepancies originate, but one possibility is that Coulwave is more dissipative than GloBouss in terms of the breaking and frictional terms, shock capturing, and numerical dissipation (time stepping). For the two time series gauges located at the more distant downstream locations G2 and F2, model differences are more distinguishable also for the leading wave train. First, it is clear that both the NLSW (non-dispersive) and the

NHESSD
2, 4857–4887, 2014

linear solutions deviate substantially from the Boussinesq formulations, clearly pointing out that both non-linear and dispersive terms should be accounted for. However, the NLSW model is still reproducing the leading wave rather well, although a slightly too early arrival and a too large amplitude is found. Second, the observed model differences between Coulwave (including inundation) and GloBouss (without inundation) are moderate, with typical amplitude deviations of 5 % for the leading wave. Therefore, run-up and dissipative effects seems to influence the wave propagation along the fjord basin, but is less significant than non-linearity and dispersion for the leading wave.

3.3 Run-up in Hellesylt and Geiranger

Using the simulation tapered at t = 7.1 s, we simulate the run-up using both Coulwave and MOST (nested with GloBouss) in Hellesylt and Geiranger. Figure 11 compares the simulated flow depths for the two models with measured data at the Hellesylt location. For Hellesylt, the topographic elevation is much less than the maximum flow depth at UH7–8 (approximately 0.001 m), whereas for at point UH6 where the topographic elevation is 0.0078 m (point UH0 is located offshore). As shown, both models estimate the first arrival of measured flow depth and surface elevation data well. However, there is a tendency that Coulwave matches the trailing waves better. Figure 12 compares the simulated flow depths for the two models with measured data at the Geiranger location. Here, the topographic elevation at the control points ranges from 0.019–0.027 m, i.e. in the same order of magnitude as the maximum flow depths. Here, large discrepancies between both models and the measured data are evident. However, the differences between simulated and measured maximum inundation (not flow depth) are still smaller than 50 % in most cases and hence somewhat less dramatic than it may seem from Fig. 12. The discrepancies are generally larger than for the corresponding Coulwave simulations where the model input is given at the F-bridge. Hence, some of the discrepancies may be carried from the offshore simulations in Coulwave and GloBouss, and not solely due to the run-up simulations themselves. The simulations using the measured data from the F-bridge as input provide a better match with the observations

NHESSD
2, 4857–4887, 2014

as shown in Fig. 7 (but with higher grid resolution), which is one indication that some of the discrepancies are caused by the propagation model. On the other hand, good correspondence between the measurements and simulations are found for one of the closest gauges (G2, Fig. 4), which indicate that offshore wave propagation is fairly well represented. Finally, there is a tendency in MOST that the inundation is reduced with increased grid resolution. An opposite tendency is found in Coulwave (Fig. 7). In general, both models largely under predict the inundation in the Geiranger location, and to a even greater extent the local water depth for the overland flow.

4 Conclusions

The present analysis has demonstrated the ability (and the lack thereof) of Boussinesq models and long wave solvers in general to tackle the demanding conditions imposed by simulating the tsunami propagation in the narrow and steep-sloping fjord system. We have used measured surface elevation measurements as input to the numerical simulations. The comparison with the wave measurements offshore has demonstrated that modeled overall characteristics such as amplitudes and wave periods are in place. As the waves (particularly the trailing ones) have different directivity, and because particle velocities measurements are lacking, improved match with data is presently difficult. However, the main purpose of this paper is to demonstrate how hydrodynamic effects influence wave propagation and run-up for characteristic wave patterns imposed by subaerial landslides in fjords. The influence of the alongshore inundation on the propagating wave has been of particular interest. Our findings suggests that the far-field propagation of landslide induced tsunamis are moderately influenced by both non-linearities and dispersion. The leading wave is surprisingly well described by the non-linear shallow water model, whereas the dispersion is clearly important for the trailing waves. We further find the inundation influences the alongshore propagation, although the effect is not very strong. As for the dispersion, the inundation seems to affect the trailing waves stronger than the leading wave.

NHESSD
2, 4857–4887, 2014

The grid resolution needed to reproduce similar waves as those imposed from the laboratory measurements are given considerable attention. From grid refinement test, we find that the resolution needed for the leading wave is at least 0.252 m, which corresponds to 125 m in real scale. For the trailing wave system, requirements are much stricter, the first 1–2 waves converge for a grid resolution of 0.126 m while the preceding waves demands higher resolution for convergence. This imposes a problem for the Boussinesq models, particularly fully non-linear operational models, as instabilities at high resolution are prominent. Therefore, our present ability to accurately model the wave train from tsunamis propagating in fjords is somewhat limited. On the other hand, the leading wave which is governing the run-up is well represented in the wave propagation simulations.

Simulated near-shore tsunami propagation and inundation at the Hellesylt location compares favorably with the measurements. The model convergence is also good at this location. For similar inundation simulations in the Geiranger location where the onshore measurement points are more distant from the shoreline, the models compare less favorable with the data, and convergence is poor. Compared to the offshore control points however, the inundation measured onshore is affected more strongly by scale effects (see Pedersen et al., 2013, for a discussion of scale effects on tsunami run-up). The viscous effects and wave breaking may for instance be influenced by the scaling, and a close correspondence with may not be expected for the overland flow. Furthermore, the friction affects the run-up (see e.g. Kaiser et al., 2011; Denissenko et al., 2014). For short the inundation distances in Hellesylt we however see that both models perform well. Seemingly more robust, MOST is able to simulate run-up at larger resolution without encountering instabilities. Comparing the two models however, we see that Coulwave are matching the flow depth equally well as MOST even though at lower resolution.

Acknowledgements. The work has been funded by the Research Council of Norway project "Laboratory experiments and numerical modeling of tsunamis generated by rock slides into fjords" (NFR 205184/F20), and by NGI.

NHESSD
2, 4857–4887, 2014

References

Blikra, L., Longva, O., Harbitz, C., and Løvholt, F.: Quantification of rock-avalanche and tsunami hazard in Storfjorden, western Norway, in: Landslides and Avalanches, ICFL 2005, Norway, Senneset, edited by: Senneset, K., Flaate, K., and Larsen, J. O., Taylor & Francis, London, UK, 57–64, 2005 4859

Denissenko, P., Pearson, J., Rodin, A., and Didenkulova, I.: Long waves climbing the slopes of different roughness: run-up height and the load on individual roughness elements, in: Proceedings of the Hydralab Joint User Meeting, Lisbon, July, 2014. 4871

Erduran, K., Ilic, S., and Kutija, V.: Hybrid finite-volume finite-difference scheme for the solution of boussinesq equations, Int. J. Num. Meth. Fluids, 49, 1213–1232, 2005. 4859

Fritz, H., Hager, W. H., and Minor, H.-E.: Near field characteristics of landslide generated impulse waves, J. Waterw. Port, Coastal, Ocean Eng., 130, 287–302, 2004. 4858

Harbitz, C., Glimsdal, S., Løvholt, F., Kveldsvik, V., Pedersen, G., and Jensen, A.: Rockslide tsunamis in complex fjords: from an unstable rock slope at Åkerneset to tsunami risk in western Norway, Coast. Eng., 88, 101–122, 2014. 4859

Harbitz, C. B., Pedersen, G., and Gjevik, B.: Numerical simulation of large water waves due to landslides, J. Hydraul. Eng., 119, 1325–1342, 1993. 4859

Heller, V., Hager, W., and Minor, M.: Scale effects in subaerial landslide generated impulse waves, Exp. Fluids, 94, 691–703, 2008. 4858

Imamura, F.: Review of tsunami simulation with finite difference method, in: Long-Wave Runup Models, edited by: Yeh, H., Liu, P., and Synolakis, C., World Scientific Publishing Co., Singapore, 25-42, 1996. 4859

Jørstad, F.: Waves Generated by Slides in Norwegian Fjords and Lakes, Institute publication 79, Norwegian Geotechnical Institute, 1968. 4859

Kaiser, G., Scheele, L., Kortenhaus, A., Løvholt, F., Römer, H., and Leschka, S.: The influence of land cover roughness on the results of high resolution tsunami inundation modeling, Nat. Hazards Earth Syst. Sci., 11, 2521–2540, doi:10.5194/nhess-11-2521-2011, 2011. 4871

Kennedy, A. B., Chen, Q., Kirby, J. T., and Dalrymple, R. A.: Boussinesq modeling of wave transformation, breaking, and run-up, Part I: 1D, J. Waterw., Port, Coast., Ocean Eng., 126, 39–47, 2000. 4863

Kim, D.-H. and Lynett, P.: Turbulent mixing and passive scalar transport in shallow flows, Phys. Fluids, 23, 016603, doi:10.1063/1.3531716, 2011. 4859, 4860, 4861

NHESSD
2, 4857–4887, 2014

Kim, D.-H., Lynett, P., and Socolofsky, S.: A depth-integrated model for weakly dispersive, turbulent, and rotational flows, Ocean Model., 27, 198–214, 2009. 4859, 4860, 4861

LeVeque, R. J. and George, D. L.: High-resolution finite volume methods for the shallow water equations with bathymetry and dry states, in: Advanced Numerical Models for Simulating Tsunami Waves and Runup, edited by: Liu, P. L.-F., Yeh, H., and Synolakis, C. E., Vol. 10, World Scientific Publishing, Third International Workshop on Long-Wave Runup Models, Catalina Island, USA, 43–74, 2008. 4859

Lindstrøm, E. K., Pedersen, G. K., Jensen, A., and Glimsdal, S.: Experiments on slide generated waves in a 1 : 500 scale fjord model, Coastal Eng., 92, 12–23, doi:10.1016/j.coastaleng.2014.06.010, 2014. 4860, 4865, 4866, 4876, 4877

Løvholt, F. and Pedersen, G.: Instabilities of Boussinesq models in non-uniform depth, Int. J. Num. Meth. Fluids, 61, 606–637, 2009. 4859

Løvholt, F., Pedersen, G., and Gisler, G.: Modeling of a potential landslide generated tsunami at La Palma Island, J. Geophys. Res., 113, C09026, doi:10.1029/2007JC004603, 2008. 4860, 4863

Løvholt, F., Pedersen, G., and Glimsdal, S.: Coupling of dispersive tsunami propagation and shallow water coastal response, Open Oceanography J., 4, 71–82, 2010. 4860, 4864

Løvholt, F., Lynett, P., and Pedersen, G.: Simulating run-up on steep slopes with operational Boussinesq models; capabilities, spurious effects and instabilities, Nonlin. Processes Geophys., 20, 379–395, doi:10.5194/npg-20-379-2013, 2013. 4859, 4861, 4863

Lynett, P.: Nearshore wave modeling with high-order Boussinesq-type equations, J. Waterw. Port Coastal Ocean Eng., 132, 2119–2146, 2006. 4863

Lynett, P., Melby, J., and Kim, D.-H.: An application of boussinesq modeling to hurricane wave overtopping and inundation, Ocean Eng., 37, 135–153, 2010. 4861, 4863

Lynett, P. J., Wu, T.-R., and Liu, P. L.-F.: Modeling wave runup with depth-integrated equations, Coast. Eng., 46, 89–107, 2002. 4859, 4860, 4862, 4863

Madsen, P. and Sørensen, O.: A new form of the Boussinesq equations with improved linear dispersion characteristics, Part 2. A slowly-varying bathymetry, Coast. Eng., 18, 183–204, 1992. 4859

Madsen, P., Bingham, H., and Schäffer, H.: Boussinesq type formulations for fully nonlinear and extremely dispersive water waves: derivation and analysis, Phil. Trans. R. Soc. Lond. A, 459, 1075–1004, 2003. 4859

NHESSD
2, 4857–4887, 2014

Miller, D.: Giant waves in Lituya Bay Alaska, Geological Survey professional paper 354-C., 1960. 4858
Nwogu, O.: Alternative form of Boussinesq equations for nearshore wave propagation, J. Waterw., Port, Coast., Ocean Eng., 119, 618–638, 1993. 4859, 4861, 4863
Oppikofer, T., Jaboyedoff, M., Blikra, L., Derron, M.-H., and Metzger, R.: Characterization and monitoring of the Åknes rockslide using terrestrial laser scanning, Nat. Hazards Earth Syst. Sci., 9, 1003–1019, doi:10.5194/nhess-9-1003-2009, 2009. 4859
Pedersen, G. and Løvholt, F.: Documentation of a global Boussinesq solver, Preprint Series in Applied Mathematics 1, Dept. of Mathematics, University of Oslo, Norway, available at http://urn.nb.no/URN:NBN:no-27775 (last access: July 2014), 2008. 4860, 4863
Pedersen, G. K., Lindstrøm, E., Bertelsen, A. F., Jensen, A., Laskovski, D., and Sælevik, G.: Runup and boundary layers on sloping beaches, Phys. Fluids, 25, 012102, doi:10.1063/1.4773327, 2013. 4871
Peregrine, D. H.: Long waves on a beach, J. Fluid Mech., 77, 417–431, 1967. 4861
Plafker, G. and Eyzagiurre, V.: Rock avalanches and wave at Chungar, Peru, Vol. 14B of Development in Geotechical Engineering, Chap. 7, 269–279, University of California, Elsevier, 1979. 4858
Sepúlveda, S. and Serey, A.: Tsunamigenic, earthquake-triggered rock slope failures during the april 21 2007 aisén earthquake, Southern Chile (45.5 degrees), Andean Geol., 26, 131–136, 2009. 4858
Shi, F., Kirby, J., Harris, J., Geiman, J., and Grilli, S.: A high-order adaptive time-stepping tvd sover for Boussinesq modeling of breaking waves and coastal inundation, Ocean Model., 43–44, 31–51, 2012. 4859
Tinti, S. and Guidoboni, E.: Revision of tsunamis occured in 1783 in Calabria and Sicily (Italy), Sci. Tsunami Haz., 6, 17–22, 1988. 4858
Titov, V. V. and Synolakis, C. E.: Modeling of breaking and nonbreaking long-wave evolution and runup using VTCS-2, J. Waterw., Port, Coast., Ocean Eng., 121, 308–316, 1995. 4859, 4864
Titov, V. V. and Synolakis, C. E.: Extreme inundation flows during the Hokkaido–Nansei-Oki tsunami, Geophys. Res. Lett., 24, 1315–1318, 1997. 4859
Titov, V. V. and Synolakis, C. E.: Numerical modeling of tidal wave runup, J. Waterway, Port, Coastal, and Ocean Eng., 124, 157–171, 1998. 4864

NHESSD
2, 4857–4887, 2014

Tonelli, M. and Petti, M.: Shock-capturing boussinesq model for irregular wave propagation, Coast. Eng., 61, 8–19, 2012. 4859

Wei, G., Kirby, J. T., Grilli, S. T., and Subramanya, R.: A fully nonlinear Boussinesq model for surface waves, Part 1. Highly nonlinear unsteady waves, J. Fluid Mech., 294, 71–92, 1995. 4859, 4861

NHESSD

2, 4857–4887, 2014

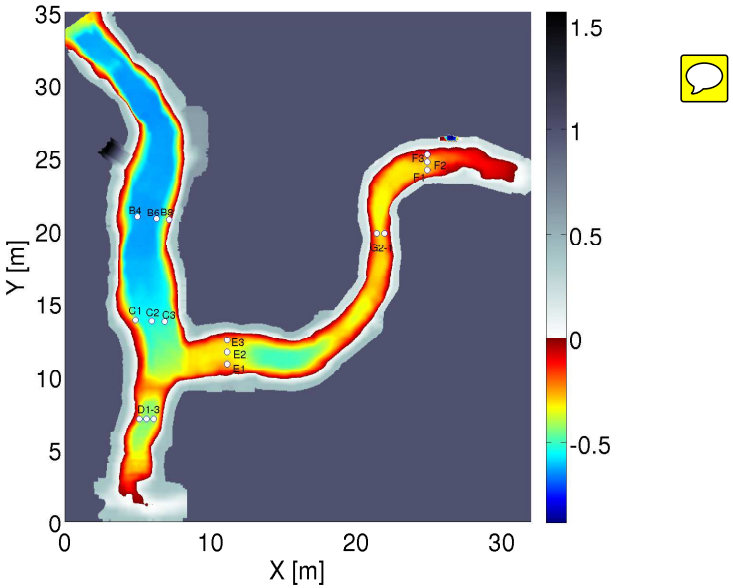

Figure 1. Applied bathymetry derived from lidar measurements of the scale model of Storfjorden. Selected locations of time series gauges that concur with the resistant wave gauges reported in Lindstrøm et al. (2014) are also depicted. The location of the landslide source in the experiments of Lindstrøm et al. (2014) is north of the B gauges (Y = 25 m).

NHESSD
2, 4857–4887, 2014

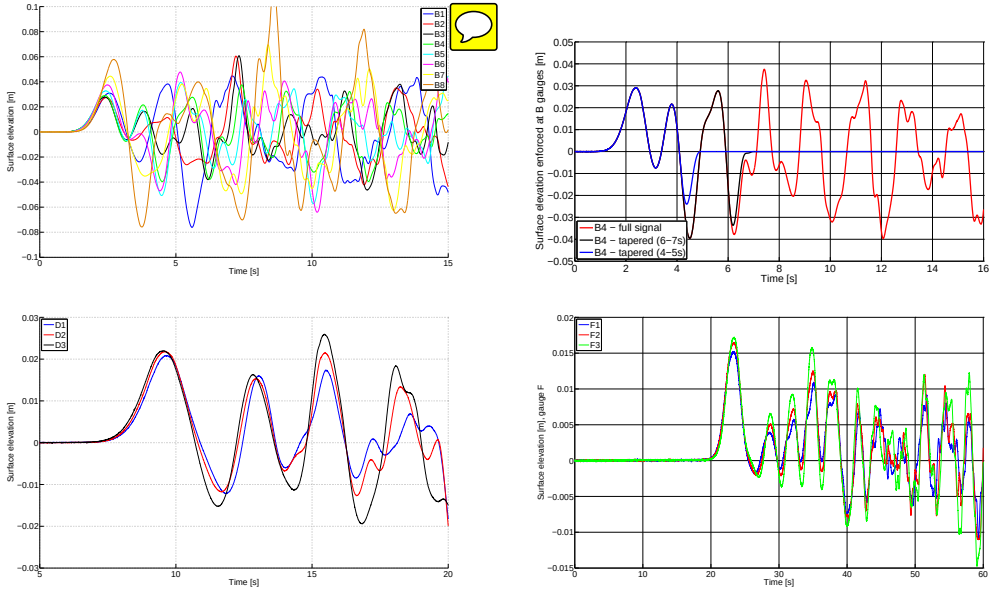

Figure 2. Upper left panel: measured surface elevations for the all the wave gauges at the B-bridge. Upper right panel: the tapered B4 signals that were used to provide input to the Coulwave simulations compared to the non-tapered signal. Lower left panel: measured surface elevations for the all the wave gauges at the D-bridge. Lower left panel: measured surface elevations for the all the wave gauges at the F-bridge. All measurement data are taken from (Lindstrøm et al., 2014).

NHESSD
2, 4857–4887, 2014

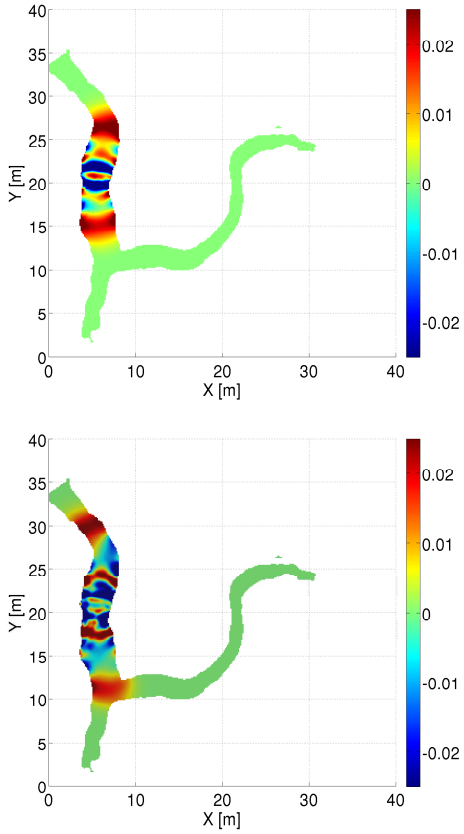

Figure 3. Initial surface elevations after wave gauge input data along the B-bridge have been tapered off. Upper panel: surface elevation after $t = 5.07$ s (B4 signal tapered between 4 and 5 s). Lower panel: surface elevation after $t = 7.1$ s (B4 signal tapered between 6 and 7 s).

NHESSD
2, 4857–4887, 2014

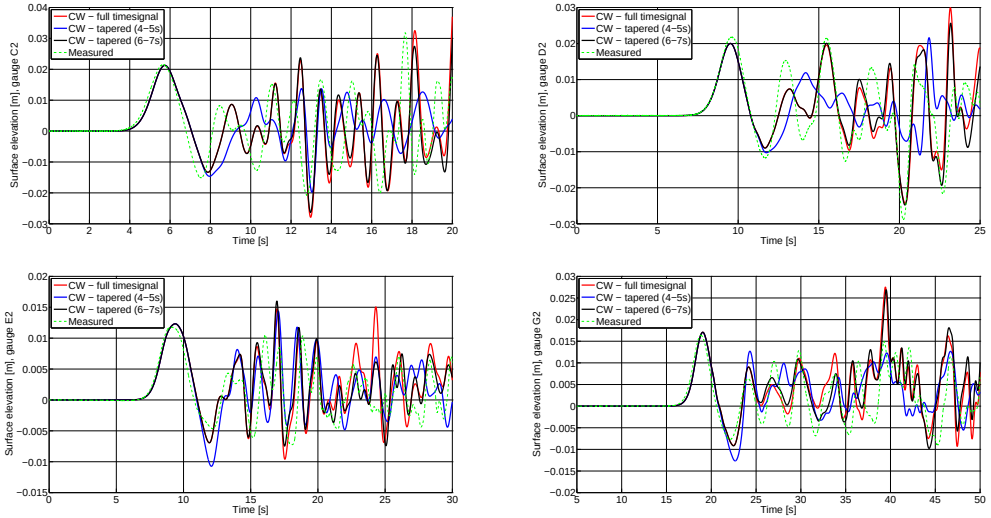

Figure 4. Comparison of the simulated surface elevations offshore using Coulwave at central gauges along the C, D, E, and G bridges. The effect of the tapering of the input signal is depicted.

NHESSD
2, 4857–4887, 2014

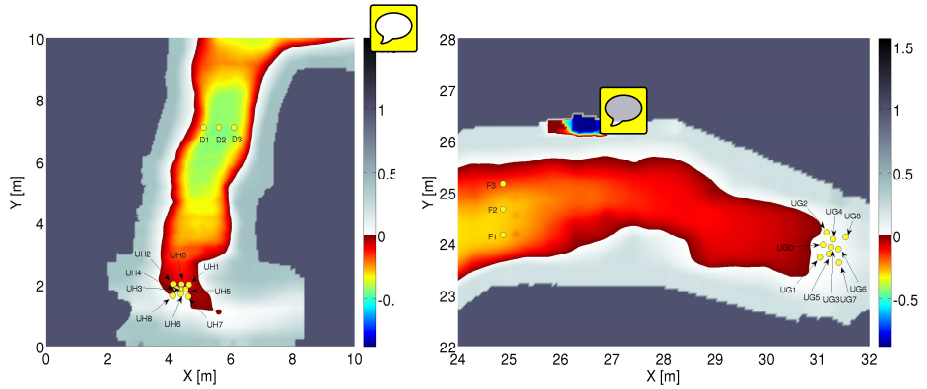

Figure 5. Left panel, location of the time series gauges for run-up computation in Hellesylt. Lower panel, location of the time series gauges for run-up computation in Geiranger.

NHESSD
2, 4857–4887, 2014

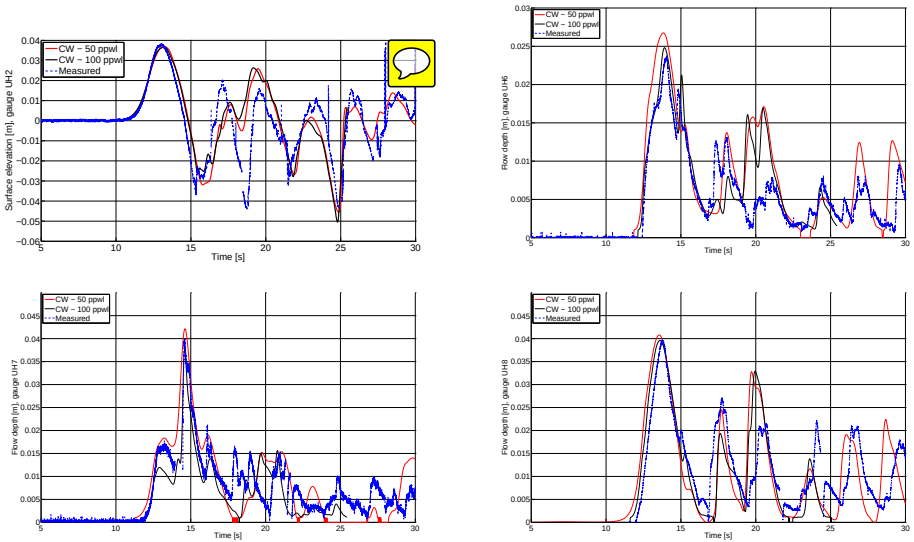

Figure 6. Simulated near shore wave evolution and inundation compared to measured signals at Hellesylt using Coulwave. The abbreviation 50 ppwl denotes a grid resolution of 0.11 m, and 100 ppwl denotes a grid resolution of 0.056 m.

NHESSD
2, 4857–4887, 2014

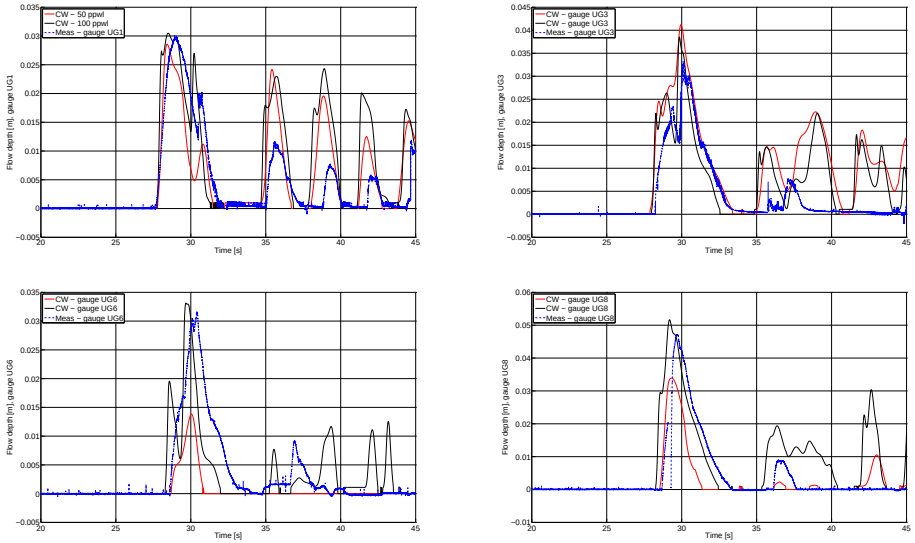

Figure 7. Simulated near shore wave evolution and inundation compared to measured signals at Geiranger using Coulwave. The abbreviation 50 ppwl denotes a grid resolution of 0.126 m, and 100 ppwl denotes a grid resolution of 0.063 m.

NHESSD
2, 4857–4887, 2014

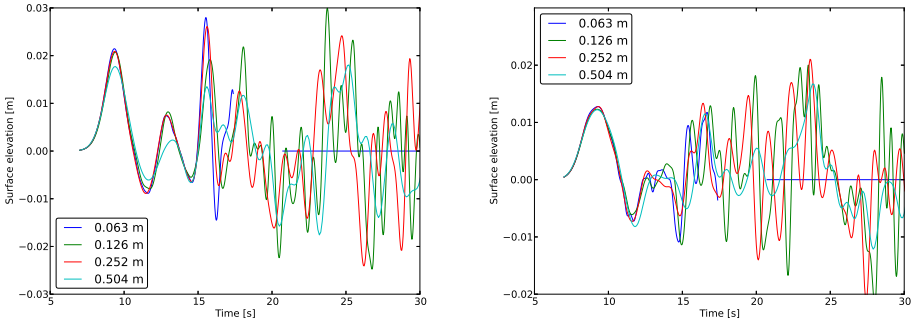

Figure 8. Convergence tests for tsunami propagation using GloBouss. The figure shows the surface elevation (mariograms) at gauges D2 (left) and E2 (right) as a function of time. The labels refer to the resolution of each simulation.

NHESSD
2, 4857–4887, 2014

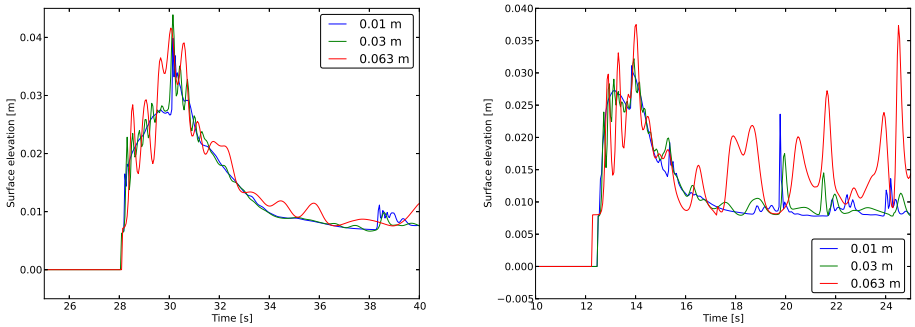

Figure 9. Convergence tests for tsunami inundation using MOST (nested with GloBouss). The waterlevel (marigrams) at gauges UG1 (left) and UH6 (right) as a function of time. The labels refer to the resolution of each simulation.

NHESSD
2, 4857–4887, 2014

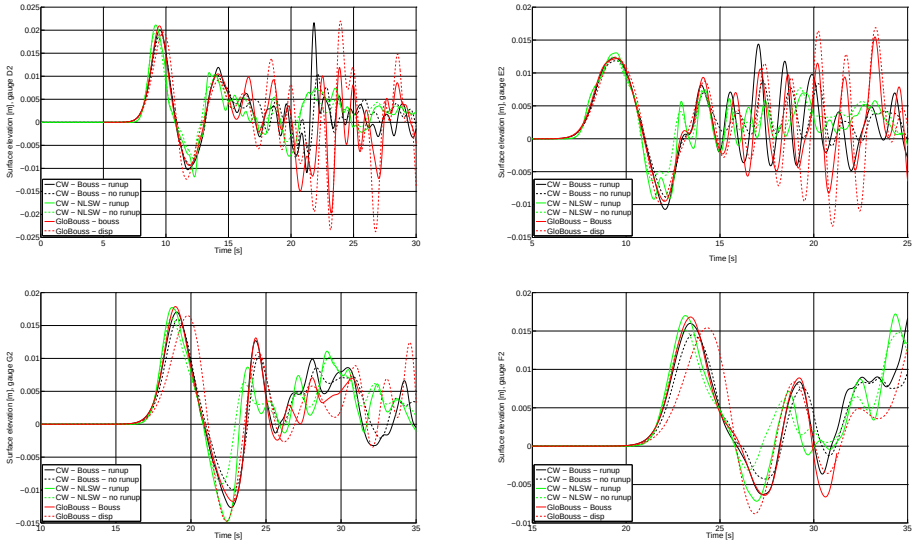

Figure 10. Comparison of the simulated surface elevations for Coulwave and GloBouss under different modeling assumptions. The abbreviation "CW" refers to the use of Coulwave. "Bouss" refers to running including both non-linear and dispersive terms in numerical model. "disp" refers to running the model in linear dispersive mode.

NHESSD
2, 4857–4887, 2014

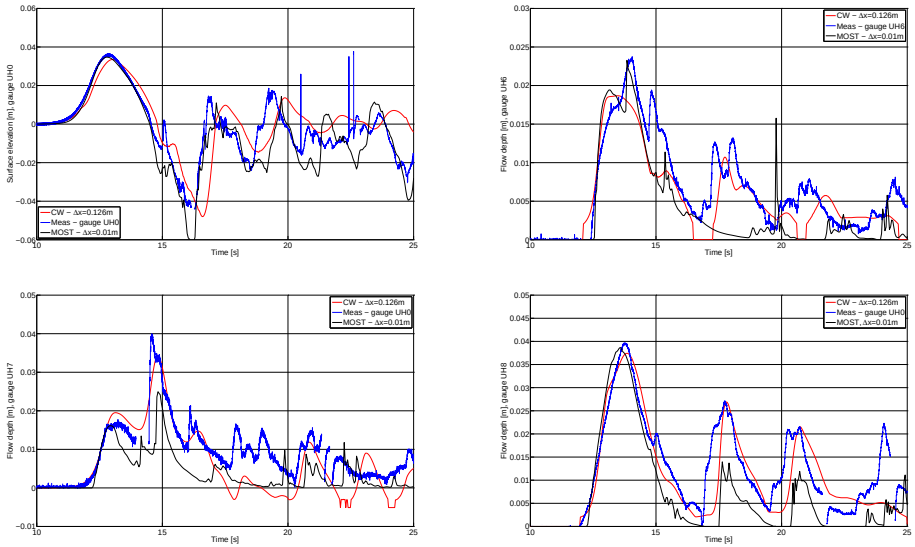

Figure 11. Simulated near shore wave surface elevation and overland flow depth in Hellesylt for Coulwave and Most.

NHESSD
2, 4857–4887, 2014

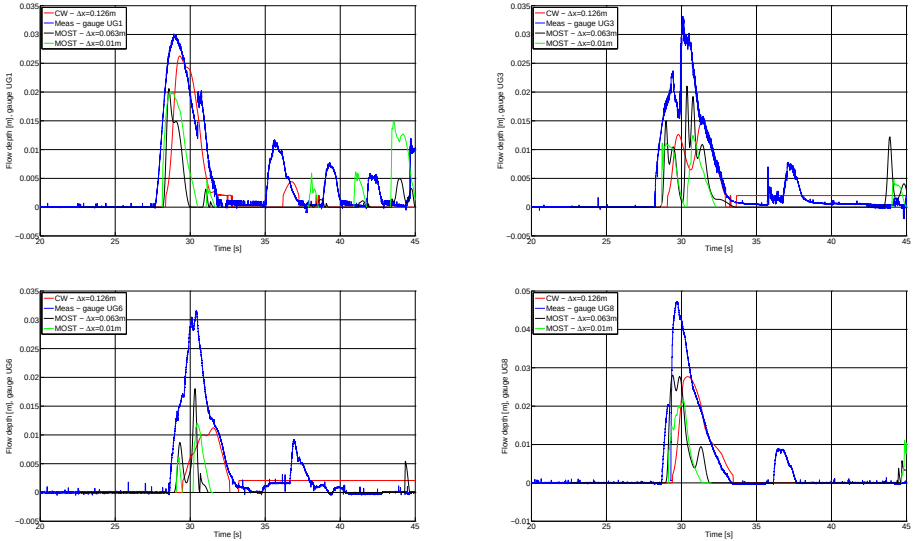

Figure 12. Simulated near shore wave surface elevation and overland flow depth in Geiranger for Coulwave and Most.

NHESSD
2, 4857–4887, 2014